ELSEVIER

Journal of Structural Geology 28 (2006) 1019–1027

JOURNAL OF STRUCTURAL GEOLOGY

www.elsevier.com/locate/jsg

Analysis of non-striated faults in a recent extensional setting: the Plio-Pleistocene Concud fault (Jiloca graben, eastern Spain)

L.E. Arlegui [a,*], J.L. Simón [a], R.J. Lisle [b], T. Orife [b,c]

[a] *Dep. Geología, Universidad de Zaragoza. Pedro Cerbuna, 12, 50009 Zaragoza, Spain*
[b] *Laboratory for Strain Analysis, Department of Earth, Ocean and Planetary Sciences, Cardiff University, UK*
[c] *Now at BG International, Reading, UK*

Abstract

The integration of palaeostress results obtained from the analysis of non-striated faults and joints affecting Plio-Pleistocene deposits near the Concud fault (southern Jiloca graben, eastern Spain) yields a multidirectional tension stress field (vertical σ_1, $\sigma_2 \approx \sigma_3$) where the primary σ_3 trajectories trend ENE. The results also show strong deflections of stress trajectories, with many local σ_3 axes being either orthogonal or parallel to the trace of the Concud fault. The stress field persisted throughout the period of activity of the fault, i.e. Late Pliocene and Pleistocene. The agreement between the present results and the regional picture gives support to the stress inversion method and shows its usefulness in palaeostress analysis of young, poorly lithified rocks.

Keywords: Stress inversion; Stress field; Stress deflection; Normal fault; Jiloca graben

1. Introduction

Palaeostress reconstruction is often hampered by the lack of striated faults in sufficient number for analysis by conventional stress inversion procedures. A new method of stress inversion based solely on observations of fault plane orientation and slip sense has been proposed by Lisle et al. (2001) and Orife et al. (2002), which permits stress interpretation in unlithified clastic deposits where striations are usually absent. This method has now been applied to fracture samples measured in Late Pliocene and Pleistocene alluvial materials of the Teruel and Jiloca grabens (Arlegui et al., 2005). The resulting picture for the most recent stress field in the region agrees well with the Miocene–Early Pliocene stress field inferred from striated faults (Simón, 1989; Cortés, 1999).

The goal of the present work is a more intensive application of this new method to non-striated fracture samples collected in the area surrounding the Concud fault (Jiloca graben, eastern Iberian Chain). The results are then compared and integrated with data obtained from extensional fractures collected at the same sites in order to achieve a more precise model of stress distribution around the fault and to check the reliability of the method. The surveyed deposits range from Late Miocene to Pleistocene in age. A number of fracture datasets were collected from previous studies in which those non-striated faults could not be adequately treated (Simón, 1983, 1989; Simón and Soriano, 1993), whereas other data sets have been collected in new dedicated field surveys.

2. Geological setting and macrostructure of the study area

The Iberian Chain is an intraplate, NW–SE-trending chain resulting from the inversion of the Mesozoic Iberian Basin. During the Palaeogene and Early Miocene, the region was compressed along two main directions (SE–NW and NNE–SSW, parallel and orthogonal to the basin trend, respectively). During the Neogene, the eastern margin of the Iberian Peninsula became dominated by the influence of rifting in the Valencia Trough (Álvaro et al., 1979). As a consequence, a large network of Neogene–Quaternary extensional basins are developed at the eastern Iberian Chain, which represent the onshore deformation of the rift (Roca and Guimerà, 1992). Driven by both rifting processes and crustal uplift, those basins evolved through two distinct episodes (Simón, 1982, 1983). The first (Miocene) produced the NNE–SSW-trending Teruel graben under well defined WNW–ESE σ_3 trajectories. The second (Late Pliocene–Quaternary) created the NNW–SSE-trending Jiloca graben and gave rise to reactivation of the Teruel graben.

* Corresponding author. Tel.: +34 976 76 21 27; fax: +34 976 76 11 06.
E-mail addresses: arlegui@unizar.es (L.E. Arlegui), jsimon@unizar.es (J.L. Simón).

0191-8141/$ - see front matter © 2006 Elsevier Ltd. All rights reserved.
doi:10.1016/j.jsg.2006.03.009

The regional stress field responsible for extensional faulting in the eastern Iberian Chain is relatively well known (Simón, 1989; Cortés, 1999). It is a nearly 'multidirectional' tension (σ_1 vertical, $\sigma_2 \approx \sigma_3$) with σ_3 trending near ENE, albeit with frequent deflections, σ_3 veering to become either parallel or perpendicular to NNW and NNE major faults. However, palaeostress determinations in the neighbourhood of the Concud fault are very scarce, mainly because the abundant fractures in this area seldom display striations, effectively disabling most of the usual methods of stress inversion. Results from fault slickenlines are limited to one site studied by Simón and Soriano (1993) in Turolian (Upper Miocene) limestones.

The Jiloca graben (Fig. 1) constitutes a large intramontane topographical depression with a smooth bottom at about 1000 m bounded by ranges and plateaus at 1200–1500 m. The Quaternary and present-day geomorphological evolution of the graben shows the prevalence of sedimentation over fluvial incision as well as the persistence of internal drainage (Rubio, 2004). The central Jiloca basin contains a Late Pliocene–Pleistocene sedimentary sequence made up of alluvial fan, pediment and episodic palustrine deposits. This sequence overlies a carbonate unit (not cropping out at the surface but observed in numerous boreholes) that could represent a Late Miocene–Early Pliocene lacustrine stage at a small precursor basin within its central sector (Rubio, 2004). In the southern sector, where the present study is focused, the recent infilling is represented by a rather complete syntectonic sequence belonging to the Pliocene (lacustrine carbonates, red clastic sediments and Villafranchian pediments) and the Pleistocene (terraces and alluvial fans spreading from the fault scarps) (Simón, 1983; Moissenet, 1985).

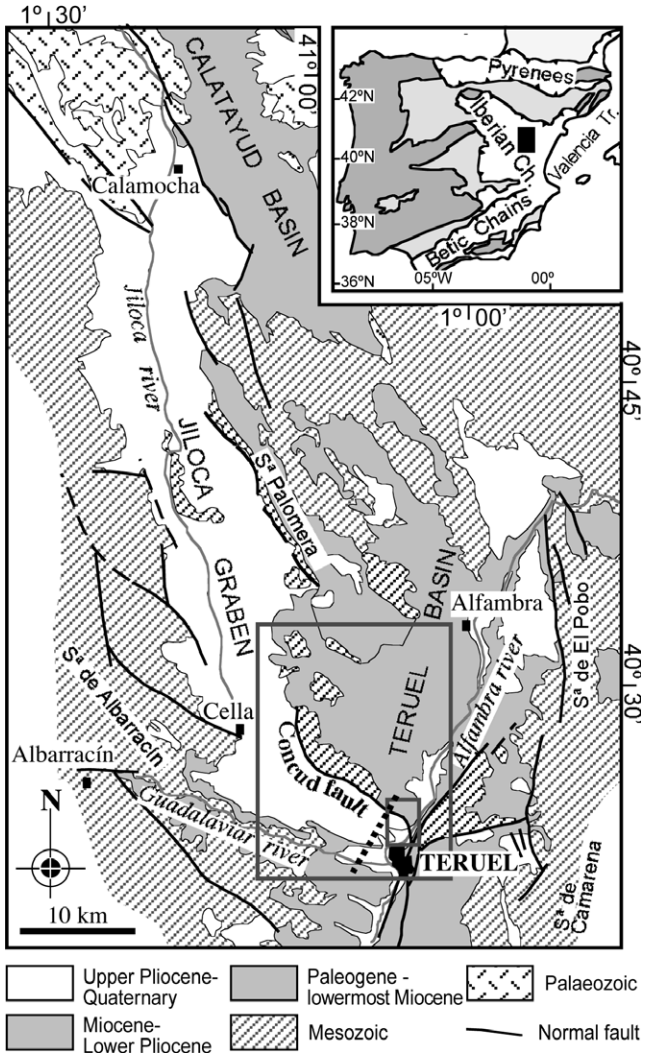

Fig. 1. Location of the study area. Rectangles correspond to Figs. 4 and 5. Dashed line indicates the cross-section in Fig. 2.

The overall NNW–SSE trend of the Jiloca graben results from an en-échelon, right releasing arrangement of NW–SE striking normal faults, the largest of which (Calamocha, Sierra Palomera and Concud faults) are located at the eastern boundary (Fig. 1). The Calamocha and Concud faults cross-cut the Miocene–Lower Pliocene lacustrine deposits of the Calatayud and Teruel basins, respectively, which allows precise calculation of their maximum offsets. In the central sector, tectonic uplift of Sierra Palomera has been interpreted from morphostructural reconstruction of the tilted block, which separates the Teruel and Jiloca grabens (about 350–400 m, similar to the height of the Sierra Palomera mountain front).

The Concud fault, at the southern sector of the Jiloca graben (Fig. 1), is about 20 km long and shows an overall NW–SE strike veering to N–S at both tips. In the hanging-wall, Lower Pliocene carbonates belonging to the Teruel basin appear at 920–940 m (Fig. 2 and map of Fig. 5), lying unconformably beneath the Upper Pliocene and Pleistocene red clastic sediments of the Jiloca graben (Godoy et al., 1983). In the footwall, the same unit forms a structural plain at 1180–1200 m. This indicates a post-Early Pliocene vertical offset of about 250 m. An independent calculation can also be made for Pleistocene times at Los Baños section (boxed area in Fig. 5), where the Concud fault offsets a fluvial terrace of the River Alfambra by some 40–60 m (Moissenet, 1985; Simón and Soriano, 1993).

3. Methodology

Lisle et al. (2001) show that the dip-slip component on a fault with dip angle γ indicates the sign of the gradient of the normal stress σ/γ. Such information, if available for differently oriented fault planes (independently of whether they are new or reactivated), allows the orientation of principal stress axes to be constrained. The procedure basically involves a comparison of the levels of normal stress calculated for the observed fault with that calculated on a slightly steeper-dipping imaginary fault plane. A grid search method then allows compilation of all stress tensors compatible with the observed faults and their respective slip senses. As a consequence of the 'reduced information content' of slip sense data when it is compared with slip vector data, a high number of compatible stress solutions is usually found. Modal orientations of the respective principal stress axes are shown on stereoplots, while stress ratios $R=(\sigma_2-\sigma_3)/(\sigma_1-\sigma_3)$ are usually displayed in the form of a frequency histogram (Orife et al., 2002).

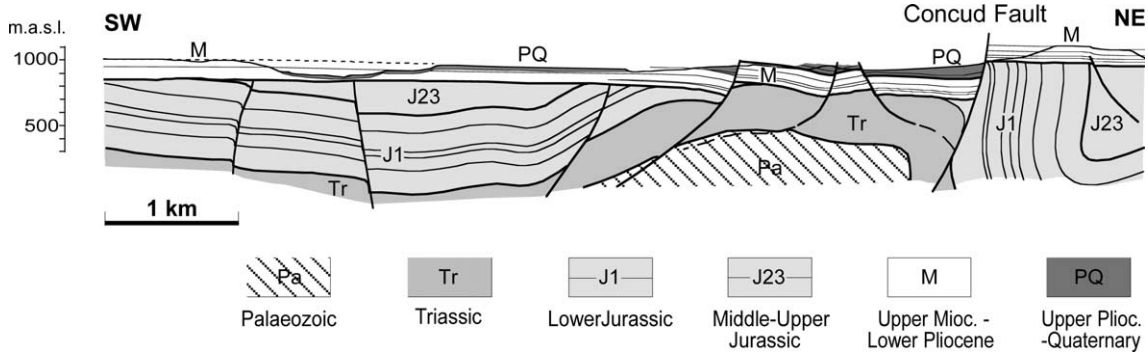

Fig. 2. Cross-section at the SE sector of the Concud fault (see location in Fig. 1).

Palaeostress analysis has been applied to samples of faults and fractures collected at 19 sites in the vicinity of the Concud fault (see Table 1). Most of the studied outcrops show clastic rocks of continental origin, mainly conglomerate and siltstone deposits formed in alluvial fans and pediments from Late Miocene to Late Pliocene in age. Other sites show Turolian (Late Miocene) lacustrine carbonates or Pleistocene fluvial terraces including gravel, sand, silt or calcareous tufa.

Five types of structures were observed. (1) Fault surfaces showing mesoscopic dip separations, with normal sense in all cases (Fig. 3). (2) Fractures with negligible offset on a mesoscopic scale, but showing normal-sense small-scale shear indicators: millimetre-scale dip separations, minor Riedel fractures or rotated pebbles. (3) Fractures without any sign of movement, interpreted as 'normal' shear or hybrid fractures on the basis of geometrical criteria: conjugate sets, smooth surfaces parallel to fractures of types 1 and 2, or angles with bedding under 75°. (4) Pure extensional joints, irregular surfaces nearly orthogonal to bedding. (5) Ambiguous fractures whose classification as either type 3 or 4 was not possible from field observation.

A dataset containing the orientations of several tens of fracture planes was collected in each outcrop, discarding in all cases those fractures belonging to type 5. Extensional joints (type 4) have been analysed separately at outcrops where a sufficient number of planes could be measured. Local σ_3 axes have been interpreted as being orthogonal to significant joint sets at those sites.

Faults and shear fractures (types 1, 2 and 3) have been considered for the inversion method of Lisle et al. (2001), with sample sizes ranging from 8 to 50. According to the description in the above paragraph, a normal sense has been input for every fracture. Stress inversion has been carried out assuming that all fractures within each sample represent a single stress episode. Actually, the method of Lisle et al. (2001) does not permit the identification of separate stress tensors that could eventually be recorded at the same site. Neither do we consider a previous

Table 1
Results of palaeostress analysis. Site 16 was studied by Simón and Soriano (1993) using the method of Etchecopar et al. (1981). See text for further explanation

N.	Lithology	Age	Stress analysis from faults			Stress analysis from extensional fractures	
			No. of data	σ_1	σ_3	No. of data	σ_3
01	Siltstone, conglomerate	Late Pliocene	28	Vertical	00, 253	8	075
02	Siltstone, conglomerate	Late Pliocene	26	Vertical	00, 065	9	070
03	Conglomerate	Late Pliocene	26	Vertical	00, 246		
04	Conglomerate	Late Pliocene	39	Vertical	00, 180	21	155
05	Gravel, silt	Middle Pleistocene	35	Vertical	00, 253		170
06	Gravel, sand	Early Pleistocene	22	Vertical	00, 126		
					00, 216	13	075
07	Gravel, silt	Late Pliocene	50	Vertical	00, 022	16	165
08	Limestone	Late Miocene	12	75, 020	16, 146		
09	Conglomerate	Middle Pleistocene	12	Vertical	00, 057		
10	Limestone	Late Miocene	8	75, 000	15, 255		
11	Limestone	Late Miocene	11	71, 067	18, 251		
12	Limestone	Late Miocene	13	70, 090	16, 195		
13	Limestone	Late Miocene	11	85, 275	05, 175		
14	Limestone	Late Miocene	16	Vertical	00, 090		
15	Gravel, sand	Early Pleistocene	13	Vertical	00, 042		
16	Limestone	Late Miocene	22	Vertical	00, 035		
17	Conglomerate	Late Miocene	33	Vertical	00, 065	18	160
18	Silt	Early Pleistocene	20	Vertical	00, 166		
19	Gravel, silt	Mid. (Late?) Pleist.	23	Vertical	00, 066		

Fig. 3. View of faults analysed in site 2.

separation of fractures (e.g. based upon the geometry of planes) as an adequate strategy. We should not discard the possibility of having 'polyphase' data sets, from which only an average stress state could have been obtained.

A number of striated faults were also observed in some outcrops of Neogene carbonates, but unfortunately the sample sizes were not large enough to provide reliable solutions. No further palaeostress result, other than that by Simón and Soriano (1993; site 16), could therefore be obtained from analysis of fault slickenlines. This prevents our testing the new method against those from 'conventional' methods in the study area, though such a comparison has previously been made for the ensemble of the Teruel and Jiloca grabens (Arlegui et al., 2005). In such a situation, analysis of tensile fractures provides the only independent way for checking the solutions obtained by the method of Lisle et al. (2001).

4. Palaeostress results. Interpretation and discussion

The obtained results of palaeostress analysis are shown in Table 1 and Figs. 4–6. Stress states inferred using the method of Lisle et al. (2001) have in all cases vertical or near vertical σ_1 axes, which is to be expected with normal faults. On the whole, the σ_3 axes have a NE–SW trend, but a closer look reveals variations as discussed below. Unfortunately, the stress ratios show very high dispersion, which gives rise to unreliable solutions, and they have therefore not been included in Table 1. Nevertheless, most stress solutions suggest a multidirectional tension regime, since the spectrum of compatible σ_3 axes obtained for each sample is widely distributed over the horizontal plane.

The arrows on maps of Figs. 4 and 5 indicate the modal azimuth of compatible σ_3 axes at each data site. Two mutually orthogonal solutions can be distinguished at site 6, which suggests σ_2/σ_3 axial switching. Two near-orthogonal white arrows show also the average solutions for sites 10–14 in Fig. 4, located close to each other within a single outcrop (a more detailed analysis is discussed in the next section; see Fig. 6). The result obtained by Simón and Soriano (1993) from striated faults is also included (site 16).

The trends of σ_3 axes show three different patterns: (a) ENE-trending axes inferred from dominantly NNW–SSE striking fractures (sites 1–3, 5, 10, 17 and 19). (b) ENE–NNE-trending axes, nearly orthogonal to the Concud fault trace, inferred from fracture samples with varied strikes (sites 6, 7, 9–11 and 14–16). (c) SE–SSE-trending axes, almost parallel to the Concud fault trace, also inferred from complex fracture patterns (sites 6, 8, 13 and 18). The N–S-trending σ_3 axes inferred at sites 4 and 12 are the only solutions not included in those patterns.

The orientations of pure tensile fractures, as shown in the rose diagrams of Figs. 4 and 5, generally agree with the former results. The NNW–SSE striking sets at sites 1, 2, 7 and 17 are consistent with well defined ENE–WSW-trending σ_3 axes, i.e. one of the stress patterns inferred from shear fractures. In the case of site 4, the dominant set strikes NE–SW, which indicates a NW–SE-trending σ_3 axis nearly parallel to the Concud fault trace. At this site, the same dominant strike is shown by shear fractures, though the N–S-trending σ_3 axis we obtained does not coincide with the former. Finally, the azimuth distribution of tensile fractures at site 6 also fits the rather scattered solution obtained from shear fractures, which suggests multidirectional tension.

Such a stress regime had been established from the low stress ratios $R=(\sigma_2-\sigma_3)/(\sigma_1-\sigma_3)$ obtained from striated fault samples in Miocene and Lower Miocene rocks (Simón, 1989; Cortés, 1999). With respect to stress orientations, those ENE-trending σ_3 axes probably mirror the far-field extensional stress during Late Pliocene and Quaternary times, with trajectories of the maximum horizontal stress (S_{Hmax}) related to recent intraplate compression and perhaps also responsible for the general trend of the Jiloca graben (Simón, 1989; Arlegui et al., 2005). Furthermore, they are parallel to the present-day stress field that can be inferred from focal mechanisms (Herraiz et al., 2000).

Stress axes either parallel or perpendicular to the Concud fault trace should be interpreted in terms of stress deflection, the observed patterns being usual on a wide range of scales

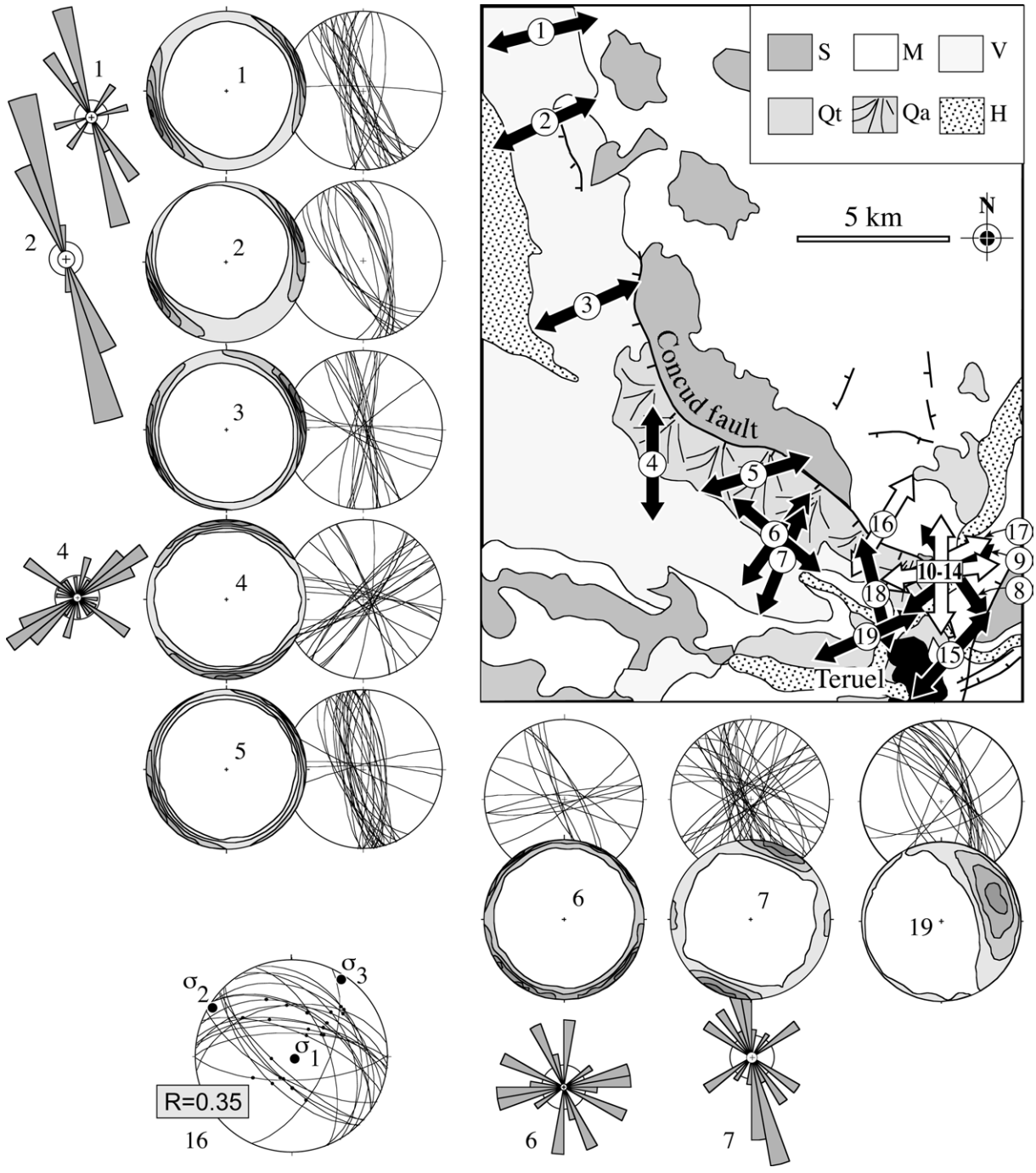

Fig. 4. Schematic geological map of the Concud fault and results of palaeostress analysis. Arrows: local directions of σ_3 axes obtained from fracture samples in Upper Miocene carbonates (white) and in clastic materials of Late Pliocene–Pleistocene age (grey); S: Mesozoic; M: Upper Miocene–Lower Pliocene; V: Villafranchian (Upper Pliocene); Qt: Pleistocene fluvial terraces and pediments; Qa: Pleistocene alluvial fans; H: Holocene deposits. Pairs of stereoplots show faults and shear fractures collected in each site and the density of compatible σ_3 axes obtained by the method of Lisle et al. (2001). Rose diagrams show strike distributions of tensile fractures. Stereoplot of site 16 includes fault planes and striae, as well as the deviatoric stress tensor obtained using the method of Etchecopar et al. (1981); $R=(\sigma_2-\sigma_3)/(\sigma_1-\sigma_3)$.

within multidirectional tension stress fields. According to the numerical models by Simón et al. (1988) and Kattenhorn et al. (2000), σ_3 trajectories run orthogonal to the strike of an extensional fault close to their tips, but parallel to it near its central zone. On the other hand, switching of σ_2 and σ_3 principal stresses, as suggested by the occurrence of two mutually orthogonal σ_3 directions at sites 6 and 10–14, is also a common phenomenon in this type of stress regime. It occurs owing to stress drop caused by the development of primary fractures, and gives rise to strain partitioning taking the form of orthogonal joint sets (Simón et al., 1988; Rives et al., 1994; Caputo, 1995; Bai et al., 2002) or pairs of conjugate normal

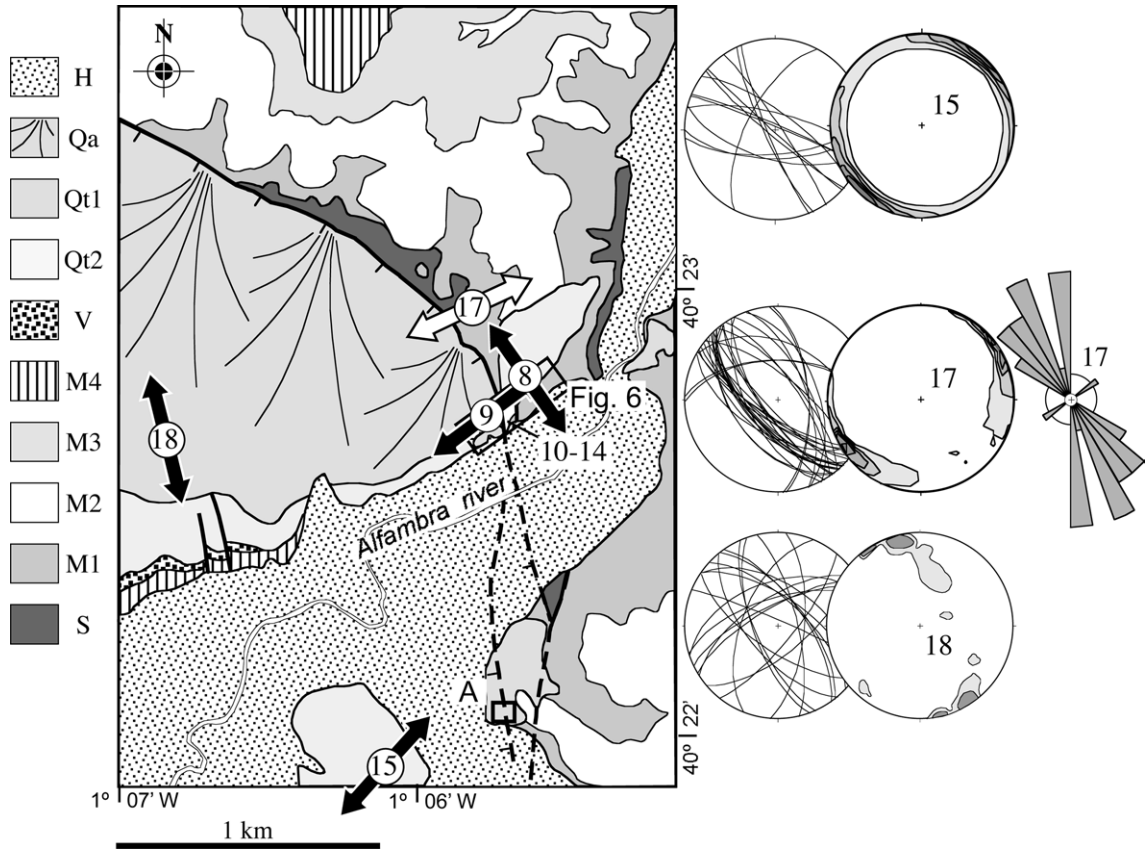

Fig. 5. Geological map of the southern tip of the Concud fault with results of palaeostress analysis. Arrows, stereoplots and rose diagrams have the same meaning as in Fig. 4. Point A corresponds to the location of Fig. 7b. S: Mesozoic; M1: Vallesian red clastic deposits; M2: Upper Vallesian–Turolien carbonates; M3: Upper Turolian clay and gypsum; M4: Ruscinian carbonates; V: Villafranchian pediment; Qt2: middle terrace; Qt1: lower terrace; Qa: Pleistocene alluvial fans; H: Holocene deposits.

fault systems striking at right angles to each other (Simón, 1989; Angelier, 1994).

5. Detailed analysis at Los Baños section (sites 10–14)

The Los Baños area, located some 3 km north of Teruel, is where more information on the Concud fault could be gathered. The main outcrop is a cutting of the old Ojos Negros–Sagunto mining railway, where the main fault and the rocks at both walls can be inspected. Fault orientation is 170°, 75° W, with a striation pitch of 75° S. As can be seen in Figs. 5, 6 and 7a, the fault brings Turolian limestones and marls in the footwall into contact with Pleistocene alluvial fan gravel and silt in the hanging wall. Turolian carbonates were strongly bent into a large monocline, then unconformably overlain with a portion of the middle terrace of the River Alfambra made up of a 5–6-m-thick layer of conglomerates topped by 1–2 m of calcareous tufa. This terrace is affected by a number of fractures and normal faults with small-offsets. Beneath the Pleistocene alluvial fan deposits of the downthrown block, there is a similar sequence of conglomerate and calcareous tufa that could represent the same fluvial terrace (Moissenet, 1985; Simón and Soriano, 1993). Height difference between both correlative deposits suggests a minimum throw of 39 m.

Most of the displacement on the Concud fault predates the lower terrace level, which appears not to be offset at Los Baños. Nevertheless, an outcrop of this terrace recently exposed by a new road near Teruel (site A in map of Fig. 5) shows a small normal fault oriented 152°, 70° W, which may record the latest propagation event of the Concud fault at its SE tip. The offset of this fault at the base of the lower terrace is 2 m (Fig. 7b), and it decreases towards the top.

The timing of the deformation can be inferred from the available age data for both of the fluvial terraces that are affected by the fault. The middle terrace has been attributed to the Middle Pleistocene on the basis of its vertebrate fauna (Godoy et al., 1983; Moissenet, 1985) and thermoluminescence dating (138 ± 10 ka; Santonja et al., 1994). This estimate has been now corroborated by analysis of Th/U isotopes in two samples collected at the centre and the top of the calcareous tufa layer at Los Baños. These have given ages of 169 ± 10 and 116 ± 40 ka BP, the second determination being the more reliable one (Table 2). The lower terrace was also attributed to the Middle Pleistocene by Moissenet (1985) on the basis of the presence of *Mammuthus trogontherii*. This age is much too close to the Th/U age of

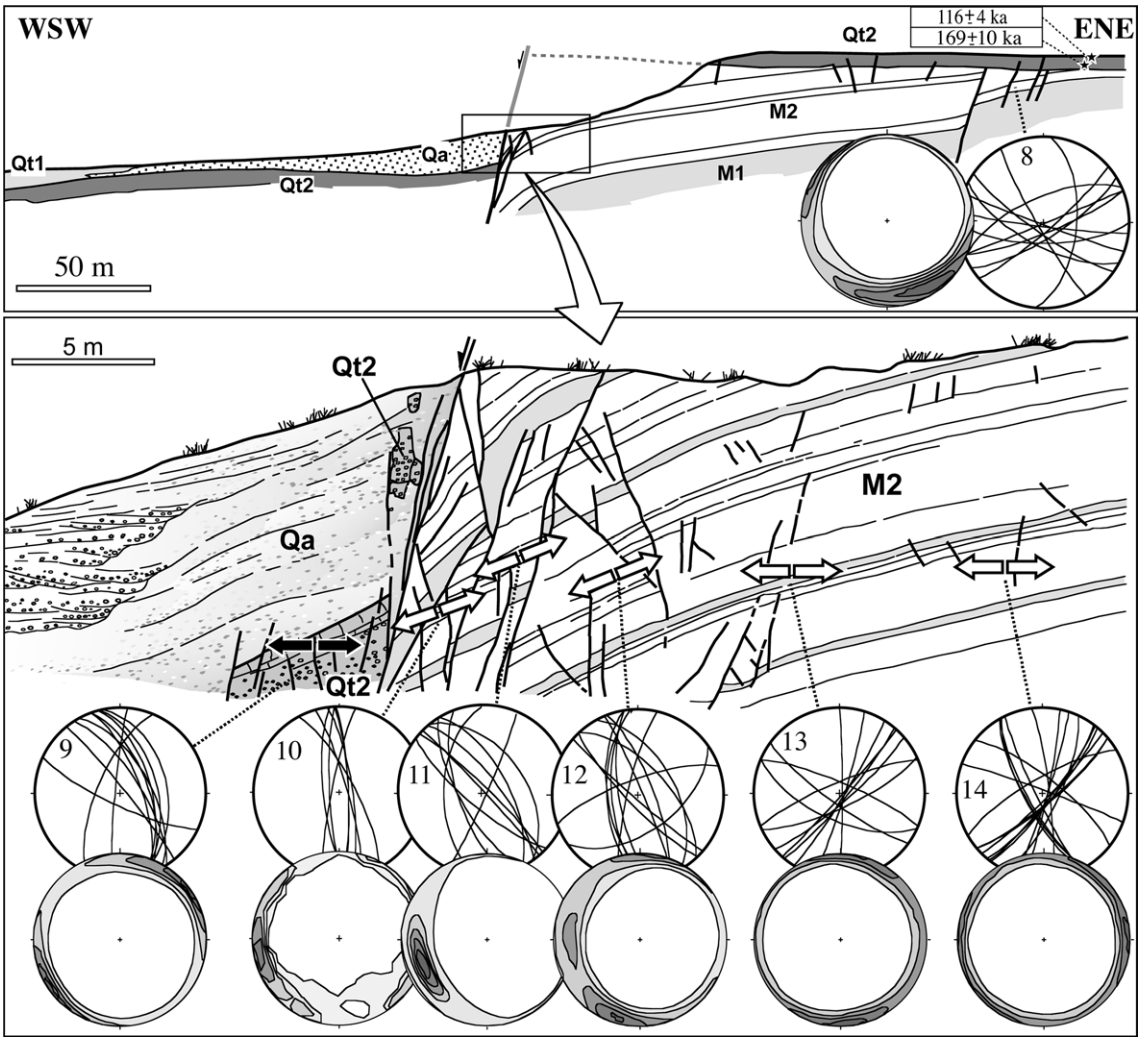

Fig. 6. The Concud fault at Los Baños section with results from palaeostress analysis. Same symbols as in Fig. 5. Arrows, stereoplots and rose diagrams have the same meaning as in Fig. 4. Arrows indicate projection of σ_3 axes on the plane of the section; true σ_3 axes are close to this plane in the case of sites 9–11 and 14, whereas they are clearly out-of-plane in the case of sites 12 and 13.

the middle terrace and probably needs revision; hence the timing of the latest event on the Concud fault remains unconstrained.

Two fracture datasets have been collected within the middle terrace conglomerates at Los Baños, one in each block, and five more within the Turolien limestones in the footwall of the Concud fault (see Fig. 6). An abundance of fractures allows us to draw fine distinctions by carefully recording where in the section the faults were collected. The results can be summarized as follows:

(1) The plunge of σ_3 axes shows varied relationships with bedding dip: σ_3 is parallel to bedding in some steeply dipping beds (sites 10–12), whereas it is almost horizontal at 9, 13 and 14, even though the beds are tilted. If we assume that the stress axes were originally horizontal, the tilted σ_3 axes should predate the monocline whereas those that are still horizontal should be younger. Such time relationships lead us to conclude that extensional fractures were initiated within the Miocene strata close to the main fault, and later—after bending had taken place—they propagated into the Quaternary levels. The stress states inferred at sites 9–14 are therefore diachronous and span much of the period during which the fault was active (Late Pliocene and Pleistocene).

(2) Stresses show heterogeneities that can be interpreted as perturbations linked to the presence of the Concud fault. On the one hand, σ_3 trajectories are deflected and tend to be perpendicular to the fault trace at sites 9–11, and parallel to it at sites 8 and 13 (the interpretation is less clear at sites 12 and 14). On the other hand, minor fracture planes are parallel to the main fault close to it (sites 9–11), and become more dispersed when we look farther from the fault, with a new orthogonal set appearing at sites 8, 13 and 14. In accordance with

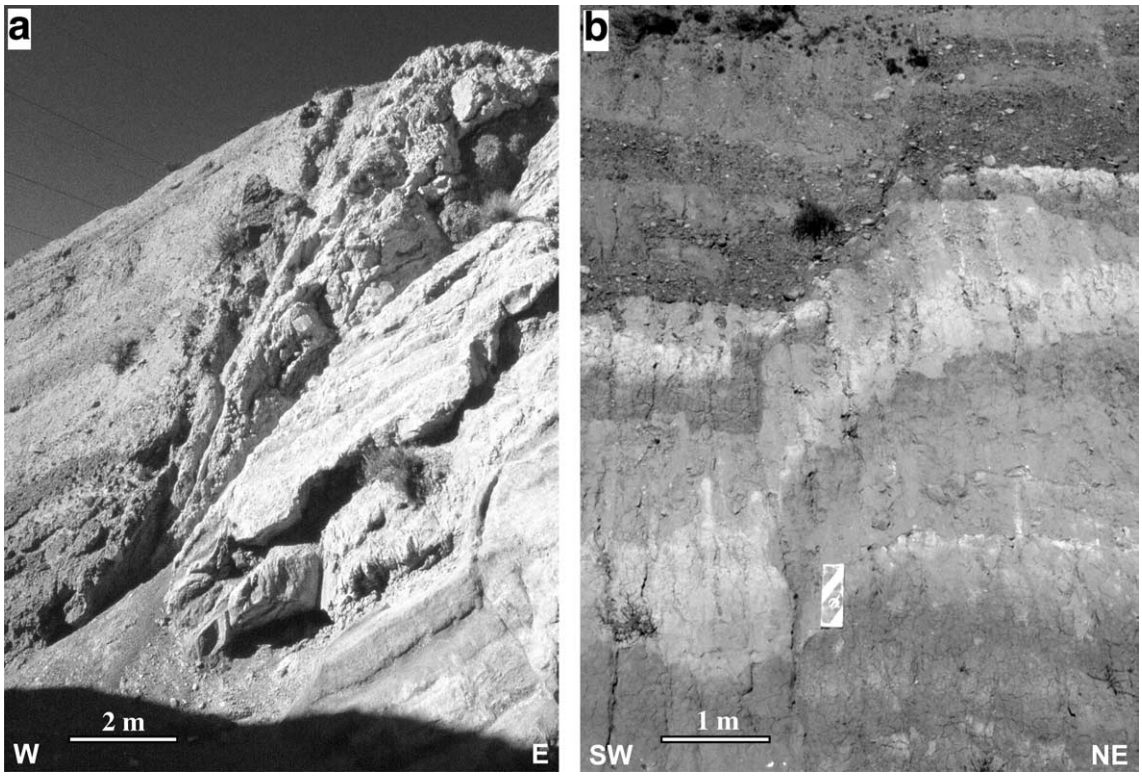

Fig. 7. (a) The Concud fault at Los Baños. (b) View of a small fault close to the southern tip of the Concud fault (site A in Fig. 5) affecting the lower terrace of the Alfambra river.

those fracture patterns, dispersion of σ_3 axes is smaller close to the fault and larger at more distant sites, which suggests that the remote multidirectional tension become more 'triaxial' within the immediate neighbourhood of the Concud fault. This change in stress ratio had also been described as an additional aspect of stress perturbation in finite-element models by Simón et al. (1988). All these stress heterogeneities seem to be basically spatial rather than temporal heterogeneities; they are clearly related to the main fault within Los Baños section, whereas they do not correlate with the timing discussed in the previous paragraph.

Table 2
Geochemical results and inferred Th/U ages for two samples collected in the calcareous tufa unit capping the middle terrace of the River Alfambra. See location in Fig. 5 (site 8) and Fig. 6 (upper cross-section). Th/U analysis carried out at the Centre d'Études et de Recherches Appliquées au Karst, Faculté Polytechnique de Mons, Belgium (May 1999)

Sample	1A	2A
Coordinates	1°05′36″ W, 40°22′54″ N	1°05′38″ W, 40°22′55″ N
Location within the unit	Middle part	Top
(U((ppm)	0.600±0.006	0.579±0.007
$^{234}U/^{238}U$	1.266±0.008	1.258±0.010
$^{230}Th/^{234}U$	0.824±0.020	0.676±0.015
$^{230}Th/^{232}Th$	7.1±0.2	15.3±0.6
Initial $^{234}U/^{238}U$	1.427	1.357
Age (ka)	169.4 (+10.0/−9.0)	115.8 (+4.6/−4.4)

6. Conclusions

The stress inversion method developed by Lisle et al. (2001) for non-striated fault surfaces allowed us to characterize the Plio-Pleistocene stress field in the vicinity of the Concud fault. Fracture data long available from clastic Late Pliocene and Pleistocene sediments allows us to complete earlier studies based on slickenline analysis (Simón, 1989; Cortés, 1999).

The stress field around the Concud fault retained a number of characteristics throughout the period of fault activity (Late Pliocene and Pleistocene). The regional stress field is basically a multidirectional tension (vertical σ_1, $\sigma_2 \approx \sigma_3$) with primary ENE–WSW-trending σ_3 trajectories, driven by a combination of intraplate remote compression, rifting and crustal uplift (Simón, 1989; Arlegui et al., 2005). Its activity has continued up to the present, as inferred from seismic focal mechanisms (Herraiz et al., 2000).

This stress field is locally perturbed by the Concud fault. In particular: (a) σ_3 trajectories are deflected, becoming either parallel or perpendicular to the fault strike; (b) there is a tendency for σ_2 and σ_3 axes to switch; and (c) the shape of stress ellipsoids evolves from multidirectional tension to triaxial tension. All these features can easily be explained by reference to theoretical models of stress perturbation within an extensional regime (Simón et al., 1988; Kattenhorn et al., 2000).

The internal coherence of the new palaeostress results and its similarity to those obtained from extensional fractures in the

same materials and sites give a measure of the soundness of the stress inversion method by Lisle et al. (2001) and of the advantages of using it in the analysis of fractures affecting recent sedimentary rocks. They also corroborate previous results (Arlegui et al., 2005) that were successfully contrasted with stress solutions inferred from striated faults in the surrounding region.

Acknowledgements

We are very grateful to C. Vita-Finci and J.M. González-Casado for their helpful and constructive reviews. Th/U analysis was carried out at the Centre d'Études et de Recherches Appliquées au Karst, Faculté Polytechnique de Mons, Belgium. Project BTE 2002-04168 of the DGES (Spanish Government) provided funding for this research.

References

Álvaro, M., Capote, R., Vegas, R., 1979. Un modelo de evolución geotectónica para la Cadena Celtibérica. Acta Geológica Hispánica 14, 172–177.

Angelier, J., 1994. Fault slip analysis and paleostress reconstruction. In: Hancock, P.L. (Ed.), Continental Deformation. Pergamon Press, Oxford, pp. 53–100.

Arlegui, L.E., Simón, J.L., Lisle, R.J., Orife, T., 2005. Late Pliocene–Pleistocene stress field in the Teruel and Jiloca grabens (eastern Spain): contribution of a new method of stress inversion. Journal of Structural Geology 27, 693–705.

Bai, T., Maerten, L., Gross, M.R., Aydin, A., 2002. Orthogonal cross joints: do they imply a regional stress rotation. Journal of Structural Geology 24, 77–88.

Caputo, R., 1995. Evolution of orthogonal sets of coeval extension joints. Terra Nova 7, 479–490.

Cortés, A.L., 1999. Evolución tectónica reciente de la Cordillera Ibérica, Cuenca del Ebro y Pirineo centro-ocidental. Ph.D. thesis, University of Zaragoza, 409pp.

Etchecopar, A., Vasseur, G., Daignières, M., 1981. An inverse problem in microtectonics for the determination of stress tensors from fault striation analysis. Journal of Structural Geology 3, 51–65.

Godoy, A., Ramírez, J.I., Olivé, A., Moissenet, E., Aznar, J.M., Aragonés, E., Aguilar, M.J., Ramírez del Pozo, J., Leal, M.C., Jerez Mir, L., Adrover, R., Goy, A., Comas, M.J., Alberdi, M.T., Giner, J., Gutiérrez Elorza, M., Portero, J.M., Gabaldón, V., 1983. Mapa Geológico de España 1:50,000, Hoja 567 (Teruel). I.G.M.E., Madrid.

Herraiz, M., De Vicente, G., Lindo-Ñaupari, R., Giner, J., Simón, J.L., González-Casado, J.M., Vadillo, O., Rodríguez-Pascua, M.A., Cicuéndez, J.I., Casas, A., Cabañas, L., Rincón, P., Cortés, A.L., Ramírez, M., Lucini, M., 2000. The recent (upper Miocene to Quaternary) and present tectonic stress distributions in the Iberian Peninsula. Tectonics 19, 762–786.

Kattenhorn, S.A., Aydin, A., Pollard, D.D., 2000. Joints at high angles to normal fault strike: an explanation using 3-D numerical models of fault-perturbed stress fields. Journal of Structural Geology 22, 1–23.

Lisle, R.J., Orife, T., Arlegui, L.E., 2001. A stress inversion method requiring only fault slip sense. Journal of Geophysical Research 106 (B2), 2281–2289.

Moissenet, E., 1985. Le Quaternaire moyen alluvial du fossé de Teruel (Espagne). Physio-Géo 14-15, 61–78.

Orife, T., Arlegui, L.E., Lisle, R.J., 2002. Dipslip: a QuickBasic stress inversion program for analyzing sets of faults without slip lineations. Computers & Geosciences 28, 775–781.

Rives, T., Rawnsley, K.D., Petit, J.P., 1994. Analogue simulation of natural orthogonal joint set formation in brittle varnish. Journal of Structural Geology 16, 419–429.

Roca, E., Guimerà, J., 1992. The Neogene structure of the eastern Iberian margin: structural constraints on the crustal evolution of the Valencia trough (western Mediterranean). Tectonophysics 203, 203–218.

Rubio, J.C., 2004. Los humedales del Alto Jiloca: estudio hidrogeológico e histórico-arqueológico. Ph.D. thesis, University of Zaragoza, 354pp.

Santonja, M., Moissenet, E., Pérez-González, A., Villa, P., Sesé, C., Soto, E., Eisenmann, V., Mora, R., Dupré, M., 1994. Cuesta de la Bajada: un yacimiento del Pleistoceno medio en Aragón. Arqueología Aragonesa 21, 61–68.

Simón, J.L., 1982. Compresión y distensión alpinas en la Cadena Ibérica Oriental. Ph.D. thesis, University of Zaragoza. Publ. Instituto de Estudios Turolenses, Teruel (1984), 269pp.

Simón, J.L., 1983. Tectónica y neotectónica del sistema de fosas de Teruel. Teruel 69, 21–97.

Simón, J.L., 1989. Late Cenozoic stress field and fracturing in the Iberian Chain and Ebro Basin (Spain). Journal of Structural Geology 11, 285–294.

Simón, J.L., Soriano, M.A., 1993. La falla de Concud (Teruel): actividad cuaternaria y régimen de esfuerzos asociado. In: Aleixandre, T., Pérez González, A. (Eds.), El Cuaternario de España y Portugal Instituto Tecnológico GeoMinero de España, Madrid 2, pp. 729–737.

Simón, J.L., Serón, F.J., Casas, A.M., 1988. Stress deflection and fracture development in a multidirectional extension regime. Mathematical and experimental approach with field examples. Annales Tectonicae 2, 21–32.